PNAS RESEARCH ARTICLE | EARTH, ATMOSPHERIC, AND PLANETARY SCIENCES

The major ion chemistry of seawater was closely coupled to the long-term carbon cycle during the Cenozoic

David Evans[a,1], Yair Rosenthal[b,c], Jonathan Erez[d], Hagar Hauzer[d,e], Laura J. Cotton[f], Xiaoli Zhou[g], Romi Nambiar[a,h], Peter Stassen[i,j], Paul N. Pearson[k], Willem Renema[l,m], Pratul Kumar Saraswati[n], Jonathan A. Todd[o], Wolfgang Müller[h], and Hagit P. Affek[d]

Affiliations are included on p. 8.

Edited by Graham A. Shields, University College London, London, United Kingdom; received May 19, 2025; accepted November 6, 2025 by Editorial Board Member John W. Valley

A ~fivefold decrease in the atmospheric concentration of CO_2 took place during the Cenozoic. This has often been viewed within the context of silicate weathering changes, although the specific contributions of the potential drivers remain poorly understood. Indeed, it has been alternatively argued that changes in the sea floor spreading rate contributed to the Cenozoic pCO_2 decline, although the magnitude of the decrease means that this is unlikely to account for the entirety of the pCO_2 change. One previously overlooked factor is the concomitant change in the major element composition of seawater, especially the concentration of calcium ($[Ca^{2+}_{sw}]$), which is typically viewed as responding to processes such as weathering, rather than representing a driver in and of itself. Here, we present the first detailed record of the Cenozoic major ion chemistry of seawater and show that $[Ca^{2+}_{sw}]$ has the potential to control key processes that impact the carbon cycle. Although our record cannot determine whether CO_2 is causally driven by $[Ca^{2+}_{sw}]$, carbon cycle box modeling identifies that this may have been the case. Whether or not $[Ca^{2+}_{sw}]$ indeed directly drove pCO_2 during the Cenozoic principally depends on the strength of the silicate weathering feedback and the magnitude of any possible changes in organic carbon burial, both of which could overwhelm a $[Ca^{2+}_{sw}]$-driven impact on the carbon cycle. As such, determining the sensitivity of the weathering–climate relationship on million-year timescales is key to resolving whether factors such as seawater major ion composition are important carbon cycle drivers.

seawater chemistry | Cenozoic CO_2 | Na/Ca | seawater calcium | foraminifera

Significance

Determining past changes in the composition of seawater is important as seawater chemistry can be thought of as an integrated record of geological processes that drive the carbon cycle. In addition, seawater major ion chemistry data are requisite information for the accurate application of many geochemical proxy systems. We provide the first record of the calcium and magnesium concentration in seawater across the early-mid Cenozoic and combine it with existing datasets to show that seawater calcium is closely correlated with atmospheric CO_2. Carbon cycle box modelling demonstrates that CO_2 may be causally driven by this aspect of seawater chemistry. If correct, we therefore identify an additional factor that may be an important driver of the long-term carbon cycle.

Over the last ~50 million years (My), Earth's climate transitioned from a greenhouse, ice-free world to an icehouse with bipolar glaciation, driven by a global mean surface temperature decrease of ~15 to 20 °C (1, 2). However, the processes that drove the ~1,500 ppm decrease in atmospheric CO_2 (3, 4) that resulted in this major climatic shift remain poorly understood. Explanations include uplift-driven changes in carbon drawdown via silicate weathering rates (5, 6), the emergence of readily weatherable (ultra)mafic arcs in the tropics (7, 8), changes in the efficiency of organic carbon production and burial (9), the evolution of key groups of calcifying plankton, and/or a shift in $CaCO_3$ deposition from platforms to the deep ocean (10, 11), or combinations thereof.

These drivers must be viewed within the context of the feedback processes that have been suggested to regulate Earth's climate within certain bounds on geologic timescales (12), and with the fact that Earth has remained habitable for billions of years. Indeed, Earth's long-term habitability is often cited as evidence for the existence of efficient feedback mechanisms (although see ref. 13). Foremost among these is the hypothesis that silicate weathering regulates Earth's climate (12, 14) via a climate/CO_2-driven change in the global weathering rate, specifically, increased weathering at higher global temperatures and vice versa. This draws down atmospheric CO_2 as (calcium) silicate rocks weathered in part by carbonic acid are buried as $CaCO_3$ in the ocean (15). While several lines of empirical evidence exist for a climatic responsiveness of silicate weathering in the geologic record (16, 17), we do not know what the slope of the relationship is (18), i.e., how sensitive silicate weathering is to global climate change. Moreover, at least in certain settings, weathering is associated with CO_2 release via the oxidation of sedimentary rock-derived organic carbon or pyrite (19). In addition, other feedback processes likely operate at climate extremes, such as at the last glacial maximum when atmospheric CO_2 possibly approached the lower limit necessary to sustain terrestrial plants (20). Overall, our understanding of Earth's long-term carbon cycle drivers and feedbacks is far from complete, while the large degree of variation in pCO_2 over the last 50 My suggests that feedbacks can only stabilize climate only within reasonably wide bounds.

Author contributions: D.E., Y.R., J.E., and H.P.A. designed research; D.E. performed research; L.J.C., P.S., P.N.P., W.R., P.K.S., J.A.T., and W.M. contributed samples; D.E. analyzed data; and D.E., Y.R., J.E., H.H., L.J.C., X.Z., R.N., P.S., P.N.P., W.R., P.K.S., J.A.T., W.M., and H.P.A. wrote the paper.

The authors declare no competing interest.

This article is a PNAS Direct Submission. G.A.S. is a guest editor invited by the Editorial Board.

[1]To whom correspondence may be addressed. Email: d.evans@soton.ac.uk.

This article contains supporting information online at https://www.pnas.org/lookup/suppl/doi:10.1073/pnas.2511781122/-/DCSupplemental.

Published January 9, 2026.

Concomitant with climatic shifts over the last 100 My was a substantial change in the major ion chemistry of seawater (21, 22), which has typically been viewed as responding to the geologic processes that drive the carbon cycle (23) rather than being a driver in itself. However, it is conceivably possible that seawater chemistry can exert a control on the carbon cycle, for example, because the saturation state of the ocean with respect to calcite (Ω_c) is proportional to the Ca^{2+} and CO_3^{2-} activity product, which is one of the key controls on $CaCO_3$ burial (10) and may also impact $CaCO_3$ production rates in the surface ocean (24). Determining whether seawater chemistry simply responds to the carbon cycle, or is a possible feedback or driver in and of itself, has been challenging because there are only a few reconstructions of past changes in seawater chemistry. From a practical viewpoint, seawater major ion data are also necessary for the application of trace element paleothermometers and the boron isotope ($\delta^{11}B$) paleo-pH proxy (3, 25). Existing records of changes in the absolute concentration of key seawater major ions (calcium, magnesium, and sulphate) are principally derived from fluid inclusions trapped in sparse marine evaporitic sequences (21, 22). Notwithstanding the importance of these datasets, the limitations of the approach are i) that $[Ca^{2+}_{sw}]$ must be indirectly inferred from $[SO_4^{2-}{}_{sw}]$ and, ii) the rare nature of these deposits means that only a handful of data points are available within the Cenozoic, at much lower resolution than the residence time of Ca^{2+} and Mg^{2+} in seawater of ~1 and ~13 My, respectively (26).

To address these limitations, we generated a new Eocene (~56 to 35 Ma) record of the major ion chemistry of seawater, at ~1 My resolution, based on the Na/Ca ratio of globally distributed, exceptionally well-preserved, shallow-dwelling large benthic foraminifera [LBF (27); see *SI Appendix*, Table S1]. Dating between 56 Ma and 31 Ma, these samples provide a continuous record of $[Ca^{2+}_{sw}]$ change through the Eocene and into the Oligocene. The basis of the approach is that the long residence time of Na^+ [>40 My (26)] means that the concentration of this ion must have been near constant over the Cenozoic (28), such that shell Na/Ca dominantly records changes in $[Ca^{2+}_{sw}]$. We combine our new LBF-derived Eocene dataset with a Neogene record derived from planktonic foraminifera (29) and couple both with existing records of the evolution of seawater Mg/Ca and Sr/Ca (30, 31) to establish Cenozoic records of the absolute concentration of Ca^{2+}, Mg^{2+}, and Sr^{2+}. Using these results and a carbon cycle box model, we explore the relationship between the concentration of calcium in seawater ($[Ca^{2+}_{sw}]$) and the carbon cycle, focusing on whether these changes may have acted to modulate pCO_2.

Results

Extensive sample characterization based on LA-ICPMS trace element analysis, mineralogy, and scanning electron microscopy (SEM) demonstrates that all samples/specimens on which our record is based are exceptionally well-preserved. All foraminifera retain their high-Mg primary mineralogy (32) and are characterized by Al/Ca <200 μmol/mol and Mn/Ca <500 μmol/mol in almost all cases. Moreover, we observe no relationship between Al/Ca or Mn/Ca and Na/Ca, nor Na/Ca and Mg/Ca or Sr/Ca on an intra- or inter-sample level, indicating no significant contribution to measured Na, Mg, or Sr from the very minor remnant clay mineral/overgrowth phases (if present; see *SI Appendix*, Fig. S4). SEM images demonstrate that all samples retain their original shell microstructure, have no diagenetic calcite in the chamber wall pores, and show no evidence of other contaminant phases (*SI Appendix*, Fig. S3).

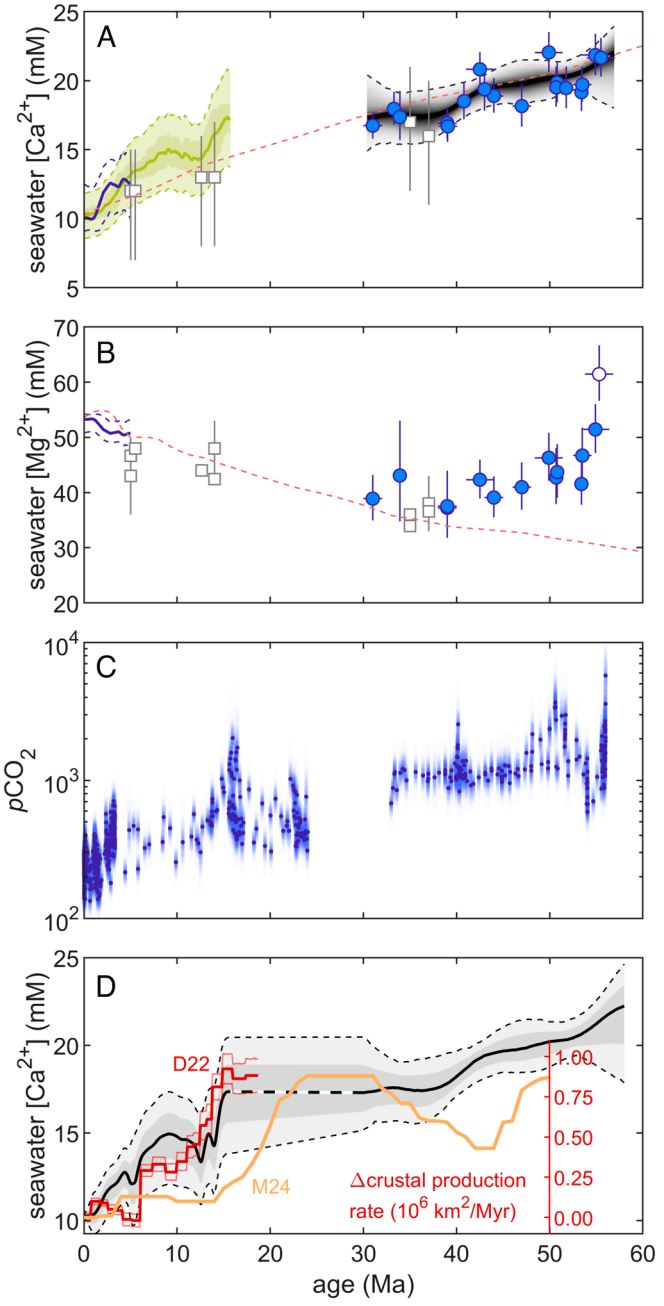

Fig. 1. Cenozoic seawater major ion reconstructions based on the Na/Ca ratio of foraminifera. (*A*) Cenozoic seawater $[Ca^{2+}_{sw}]$ reconstruction from this study, together with previous approaches (21, 22, 29, 33) and geochemical box-modeling (ref. 36, red dashed line). (*B*) $[Mg^{2+}_{sw}]$ derived from Na/Ca-derived $[Ca^{2+}_{sw}]$ and the Mg/Ca_{sw} record of ref. 31. One outlier is shown by an open symbol (at 56 Ma; see *SI Appendix*, Table S3). (*C*) $\delta^{11}B$-derived pCO_2, updated from ref. 3 using the seawater major ion record of this study, with all sources of uncertainty fully propagated via Monte Carlo simulation. (*D*) Composite Cenozoic seawater $[Ca^{2+}_{sw}]$ (black line; see *SI Appendix* for details) with estimates of changes in the global oceanic crustal production rate overlain (red and orange lines) (34, 35).

Cenozoic Calcium, Magnesium, and Sulfate Records. Our record demonstrates that Eocene $[Ca^{2+}_{sw}]$ ranged between 17.5 mM and 22.7 mM and was thus 1.7 to 2.2 times higher than at present (Fig. 1*A*), in excellent agreement with the sparse fluid inclusion data where they overlap at ~35 Ma (for details of the transformation of measured Na/Ca into $[Ca^{2+}_{sw}]$, see the *Materials and Methods* and *SI Appendix*). Moreover, the LBF-derived Na/Ca reconstruction delineates a ~4 mM (20%) decrease in $[Ca^{2+}_{sw}]$ through the Paleogene, from $20.8^{+2.0}_{-2.4}$ mM in the earliest Eocene to $17.0^{+2.1}_{-2.6}$ mM

in the early Oligocene. During the Neogene, an existing planktonic foraminifera Na/Ca-derived dataset (29) shows a further ~5 to 7 mM decrease between the mid-Miocene and present-day, such that approximately half to two-thirds of the Cenozoic decrease in $[Ca^{2+}_{sw}]$ occurred in the last 15 My. We note that the Plio-Pleistocene portion of the Na/Ca-derived $[Ca^{2+}_{sw}]$ record is in excellent agreement with an independent record based on a deconvolution of the Mg/Ca_{sw} reconstruction of ref. 33 (see *SI Appendix* for details), lending support to both approaches. The lack of Oligocene data precludes us from determining whether $[Ca^{2+}_{sw}]$ changed during this interval; while an unidentified Oligocene excursion may have taken place the indistinguishable mid-Miocene and earliest Oligocene reconstructed $[Ca^{2+}_{sw}]$ of 17.5 ± 2 mM suggests that little change occurred (Fig. 1*D*). Our composite $[Ca^{2+}_{sw}]$ record shows strong coherence with reconstructions of global crustal production rate (34, 35) where they overlap. While our data do not demonstrate a causal link between the two, this may suggest a dominant marine tectonic control on Neogene seawater chemistry, as further discussed below.

Seawater $[Mg^{2+}]$ was determined by combining our composite Cenozoic $[Ca^{2+}_{sw}]$ record with an existing Mg/Ca_{sw} dataset based on a similar sample set, wherein the effects of Mg/Ca_{sw} and temperature on calcite Mg/Ca were deconvolved using clumped isotope paleothermometry (31). Our $[Mg^{2+}_{sw}]$ record shows an overall increase since the mid-Eocene of 13 mM, consisting of a Paleogene decrease of ~5 mM before increasing to the present-day value through the Neogene (Fig. 1*B*). The structure of this dataset is significantly different from interpolation between the sparse fluid inclusion reconstructions (28), highlighting previously unidentified changes in seawater chemistry.

To provide a complete seawater major ion chemistry reconstruction, $[SO_4^{2-}{}_{sw}]$ was derived via the assumption that the product of $[Ca^{2+}_{sw}]\cdot[SO_4^{2-}{}_{sw}]$ has remained constant or within narrow bounds through geologic time, the reverse of the method used to determine $[Ca^{2+}_{sw}]$ from evaporite fluid inclusion $[SO_4^{2-}]$ (21, 22). While there is, to our knowledge, no a priori reason to think that this should have always been the case, the agreement between our Na/Ca-derived $[Ca^{2+}_{sw}]$ with the fluid inclusion data where they overlap means that this assumption appears reasonable during at least the latter half of the Cenozoic (and is consistent with alternative methods of constraining $[SO_4^{2-}]_{sw}$ (37, 38)). Finally, we determine $[Na^+]$ by maintaining charge balance following ref. (28), with the additional constraint of constant $[K^+_{sw}]$ (37), which results in calculated $[Na^+_{sw}]$ within 5% of the modern value throughout the Cenozoic, rising from 95 to 100% of the modern value during the Paleogene (*SI Appendix*, Fig. S6).

To examine the relationship between Cenozoic seawater chemistry and the carbon cycle, we first recalculate surface ocean seawater carbonate chemistry over this interval. This is necessary because $[Ca^{2+}_{sw}]$, $[Mg^{2+}_{sw}]$, and $[SO_4^{2-}{}_{sw}]$ exert a control on the carbon and boron system dissociation constants, such that $\delta^{11}B$-derived pH and pCO_2 require revision in light of our seawater major ion chemistry record (see *SI Appendix* for details of these calculations). Based on this, we solve the complete seawater carbonate system by coupling boron isotope-derived pH reconstructions with our composite $[Ca^{2+}_{sw}]$ record (Fig. 1*A*), assuming constant surface ocean calcite saturation (Ω_c) (3, 28, 39), while fully propagating all sources of error via Monte Carlo simulation (*SI Appendix*). We stress that constant Ω_c is demonstrably not the case across transient climate events (40), but Ω_c cannot change to a large degree because feedbacks in $CaCO_3$ production and dissolution act to rebalance the system on the multi-My timescales (11) relevant here.

Our revised atmospheric CO_2 record reveals that early-mid Eocene pCO_2 was ~100 to 500 ppm higher than previously reported (3), for an equivalent set of underlying assumptions (constant Ω_c), with peak pCO_2 during the early Eocene climatic optimum (EECO) of 1,200 to 3,000 ppm [Fig. 1*C*; a more recent multiproxy compilation falls within this range (4)]. Given that both pCO_2 and $[Ca^{2+}_{sw}]$ are characterized by a substantial decrease through the Cenozoic (Fig. 1), we quantify the extent to which these factors covaried. Binning the datasets into 1 My intervals removes short-term variation in the pCO_2 record that must be related to processes independent of seawater major ion chemistry, given the residence times of the seawater major ions [e.g., orbitally driven variability, transient events such as the Paleocene–Eocene thermal maximum (PETM)]. We find a tight relationship between pCO_2 and $[Ca^{2+}_{sw}]$ during much of the Cenozoic (R^2 = 0.83, P << 0.01; Fig. 2), potentially indicating a common driver. In contrast, we find no relationship between $[Ca^{2+}_{sw}]$ and total alkalinity (TAlk), although a substantial (~1,000 µmol/kg) long-term shift in TAlk may have taken place if surface ocean Ω_c covaried with $[Ca^{2+}_{sw}]$(*SI Appendix*, Fig. S11). We acknowledge that this exercise averages across transient (<1 My duration) events such as

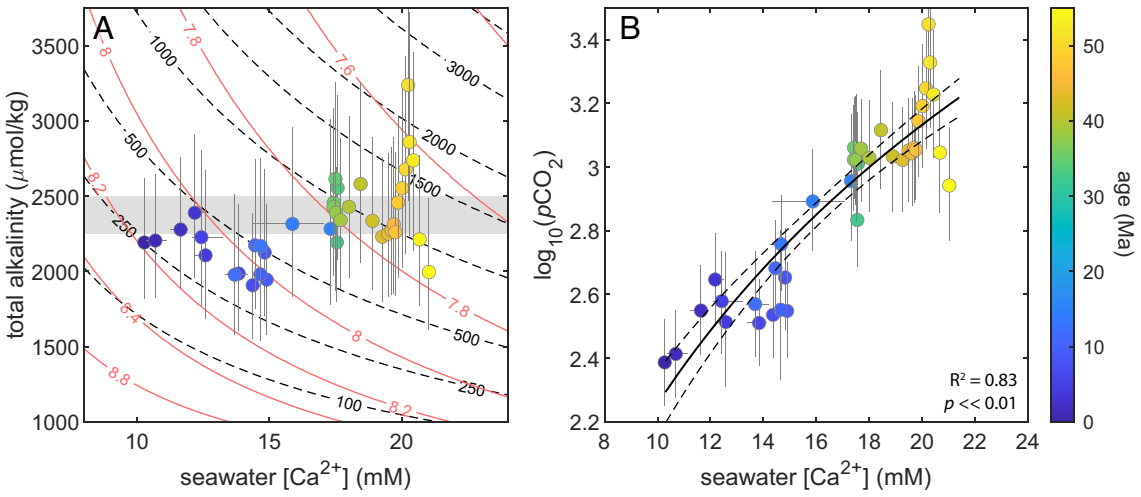

Fig. 2. The relationship between $[Ca^{2+}_{sw}]$, TAlk, and pH/CO_2, based on the data in Fig. 1, binned into 1 My intervals (symbol color reflects geologic age; scale shown on *Right*). (*A*) Given a broadly stable Ω_c over the Cenozoic (11), total alkalinity (TAlk) and $[Ca^{2+}_{sw}]$ were decoupled over this interval. Contours show the relationship between $[Ca^{2+}_{sw}]$ and pH and pCO_2 for the theoretical case that there was no change in TAlk. (*B*) Reconstructed covariation between $[Ca^{2+}_{sw}]$ and pCO_2.

the PETM, that are unlikely to have driven a substantial change in seawater major ion chemistry (<1%, see *SI Appendix*, Fig. S14 and ref. 10) but were associated with large pCO_2 changes, potentially biasing the reconstructed pCO_2 values in this 1 My bin for the purposes of our comparison. However, the sparsity of data from, for example, the core of the PETM means that this limitation does not exert a significant impact on our findings. Rather, determining whether the scatter in the early Eocene pCO_2 data represents real variability or noise (Fig. 1*C*) is more important in understanding whether this interval deviated from the overall Cenozoic pCO_2-$[Ca^{2+}_{sw}]$ relationship (Fig. 2).

Discussion

The Relationship between Seawater Major Ion Chemistry and the Carbon Cycle. Our results demonstrate that $[Ca^{2+}_{sw}]$ and pCO_2 are tightly correlated across multi-million-year timescales. However, this does not necessarily mean that there is a causal link between changing seawater chemistry and climate. For example, it is possible that a change in the global silicate weathering rate, driven by uplift or "weatherability" (5, 41), controls not only the balance between CO_2 outgassing and drawdown but also the chemistry of seawater via (e.g.) delivery of the weathering product. Likewise, a change in the global crustal production rate (34) might be expected to drive both the CO_2 outgassing rate (42) as well as $[Ca^{2+}_{sw}]$ and $[Mg^{2+}_{sw}]$ via fluid–rock interactions at mid ocean ridge hydrothermal systems (43, 44). In both cases, the major ion composition of seawater can be viewed as responding to the same underlying geologic process that drove the carbon cycle.

Alternatively, it is conceivable that $[Ca^{2+}_{sw}]$ is a carbon cycle driver in and of itself. $[Ca^{2+}_{sw}]$ exerts a primary control on the saturation state of seawater, which is in turn a likely control on the $CaCO_3$ production rate of at least some key groups of calcifying organisms such as foraminifera and corals (45, 46). In addition, Ω_c exerts a primary control on $CaCO_3$ preservation/dissolution rates in the deep ocean (e.g., ref. 47). $[Ca^{2+}_{sw}]$ may therefore impact the carbon cycle, for example, in that an Ω_c decrease driven by $[Ca^{2+}_{sw}]$ may be expected to reduce global $CaCO_3$ production in the surface ocean. Given that calcification is an instantaneous source of protons, decreased calcification could act to increase the ratio of TAlk to dissolved inorganic carbon (DIC) in the surface ocean, therefore increasing pH and $[CO_3^{2-}]$ and decreasing atmospheric CO_2. The oceanic carbon cycle is of course substantially more complex than this, with multiple interacting processes controlled by differing aspects of seawater carbonate chemistry, and we cite this as one example of a mechanism that *could* result in a $[Ca^{2+}_{sw}]$-driven CO_2 change. Indeed, alternative processes by which a change in $[Ca^{2+}_{sw}]$ could potentially influence the carbon cycle have been proposed within the context of evaporite weathering (48). Whether or not this was the case depends on the strength of other processes and feedbacks, in particular, whether changes in the global degassing or weathering rate are sufficiently large to dwarf any change that might arise from seawater major ion chemistry alone.

To test the hypothesis that $[Ca^{2+}_{sw}]$ could potentially have played a role in the evolution of Cenozoic climate, rather than simply responding to processes such as weathering or crustal production rates, we present a simple carbon cycle box model ("DeepCarb"; see *SI Appendix* for details and model validation). The computational efficiency of the model enables us to vary model parameterizations over an extremely wide range to understand the sensitivity of the model to the way it is initialized. Specifically, we randomly vary the slope of the relationship between i) silicate weathering rate and climate, ii) $CaCO_3$ production and surface ocean Ω_c, and iii) $CaCO_3$ preservation/dissolution and deep ocean Ω_c. These model perturbations are run in a Monte Carlo fashion with random permutations of these slopes, enabling us to determine the sensitivity of our box model to the way that these relationships are parameterized. The rationale for doing so is that, to our knowledge, no good constraint exists for any of these key relationships on geologic timescales. For example, the sensitivity of silicate weathering to temperature (or pCO_2) as implemented in a number of carbon cycle models varies by around an order of magnitude (18), implying, at the very least, that this is poorly constrained and/or that it varies through time (49). We stress that the model presented here cannot unambiguously constrain whether or not $[Ca^{2+}_{sw}]$ did indeed play a direct, causal role in the Cenozoic CO_2 decline, because the results of a model run in this fashion depend on how these relationships are parameterized within an individual simulation. They can, however, identify whether a mechanism exists that could plausibly result in $[Ca^{2+}_{sw}]$ driving atmospheric CO_2.

Here, the model was set up to assess whether Cenozoic pCO_2 is causally or correlatively related to $[Ca^{2+}_{sw}]$. Starting from Eocene boundary conditions, we test two key hypothesized drivers of Cenozoic climate: i) an externally driven decrease in $[Ca^{2+}_{sw}]$ ("force Ca" set of simulations; Fig. 3*D*), which could mechanistically represent (e.g.,) a change in the rate of seawater–basalt interaction (50), and ii) an increase in the silicate weathering rate (ref. 5), to determine the expected $[Ca^{2+}_{sw}]$ and seawater carbonate chemistry change in response to this process alone. In the latter case, we run the model both with and without an associated change in the $[Ca^{2+}]/[HCO_3^-]$ of the weathering product ("force SiW + SW Ca" and "force SiW" simulations respectively; Fig. 3 *C* and *E*), to assess the impact of a simultaneous change in both the degree of weathering and type of material being weathered on our results. In all cases, the model perturbation was chosen to match the approximate magnitude and rate of reconstructed (Fig. 1) changes in either $[Ca^{2+}_{sw}]$ or pCO_2, with a SiW change of ~25% required to result in a comparable magnitude of CO_2 change to that observed over the Cenozoic. Only the aforementioned parameters were forcibly perturbed (e.g., only $[Ca^{2+}_{sw}]$ was forced in the "force Ca" simulations) with all other fluxes and parameters allowed to vary freely, including the saturation state of the ocean boxes. We note that while we explore only SiW-driven pCO_2 changes, this is functionally identical to driving the CO_2 degassing rate in our box model, given that a SiW-driven change in CO_2 affects model fluxes in the same way as a CO_2-driven change in SiW (see *SI Appendix*). As such, our SiW experiments could equally represent a SiW change driven independently of climate (e.g., mountain building or the emplacement of weatherable material) or a change in the CO_2 degassing rate.

Increasing the silicate weathering rate substantially drives down pCO_2 to an extent that is strongly dependent on how the responsiveness of silicate weathering to temperature is parameterized (Fig. 3 *A* and *F*), with individual simulations with shallow SiW–CO_2 relationships characterized by larger pCO_2 changes. While unsurprising, this reinforces the need to constrain both the modern SiW–CO_2 relationship (18), how it may have changed through time (49), and whether other weathering processes contribute to CO_2 release or drawdown (19), before interpreting the output of any carbon cycle model in specific terms. More importantly however, the Monte Carlo nature of these simulations highlights emergent properties in the model which can be used to diagnose whether a model driven in this way can explain the broad features of Cenozoic carbon cycle change. The first of these is that no parameterization of the key relationships explored here is capable of driving any substantial change in $[Ca^{2+}_{sw}]$ (Fig. 3*C*). This is because the

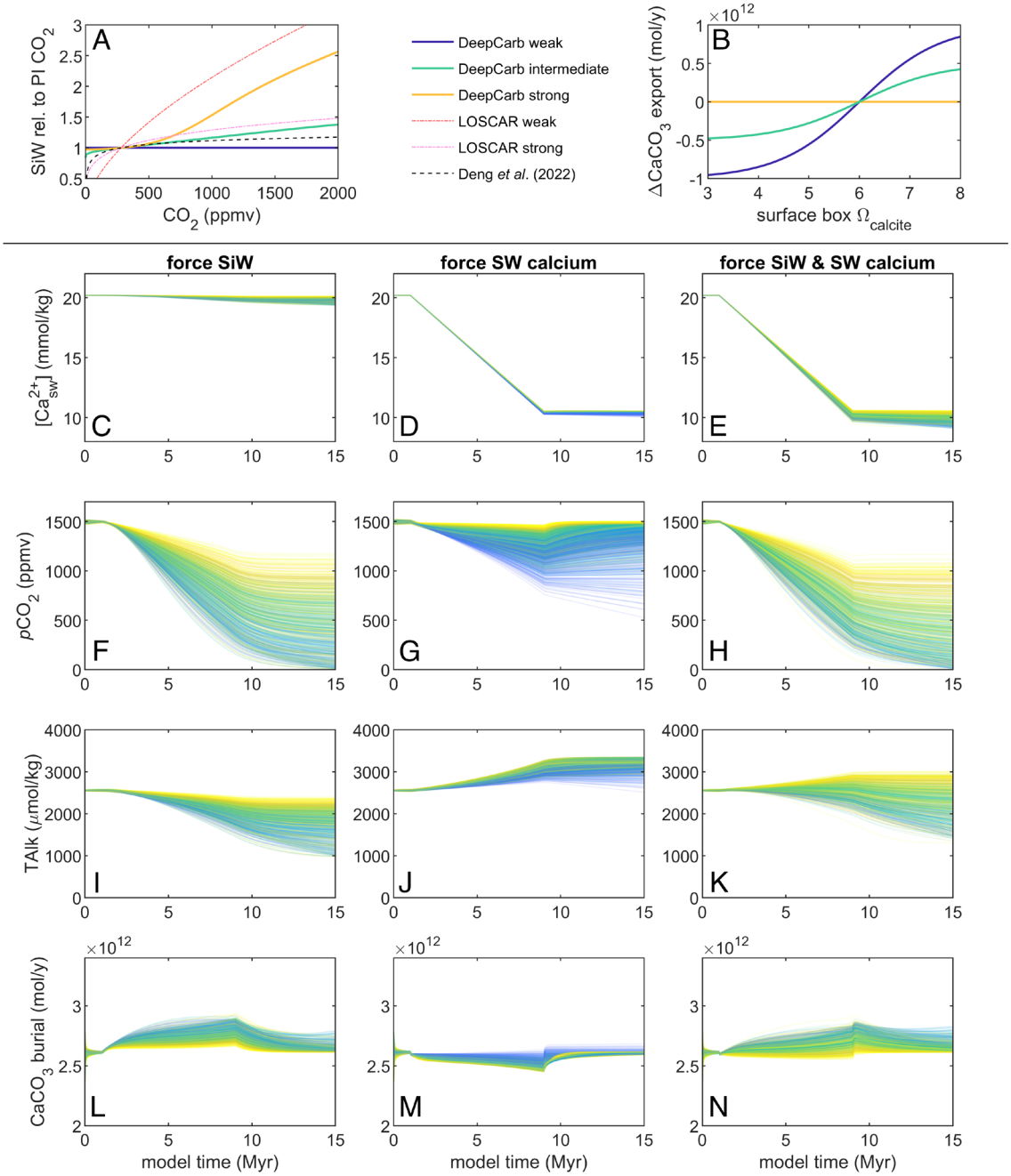

Fig. 3. The effect of silicate weathering on $[Ca^{2+}_{sw}]$, and $[Ca^{2+}_{sw}]$ on pCO_2 in a carbon cycle box model. (*A*) Silicate weathering (SiW)-climate relationships as implemented in *DeepCarb* (this study) and LOSCAR (18), with a modern empirical estimate shown for comparison based on the SiW–temperature relationship of ref. 51 coupled with the same CO_2–temperature relationship as implemented in *DeepCarb*. We stress that the assumption that a relationship based on modern regional heterogeneity is equivalent to the effect of global climate change on geologic time is highly uncertain such that this comparison is intended to be illustrative only. (*B*) The range of surface ocean Ω_c–$CaCO_3$ export slopes implemented in *DeepCarb*. (*C*–*N*) *DeepCarb* model results. (*C*, *F*, *I*, and *L*) The evolution of $[Ca^{2+}_{sw}]$, pCO_2, TAlk, and $CaCO_3$ burial in 1000 *DeepCarb* simulations in which the SiW–CO_2 relationship was increased by 25% over 8 My (starting at 1 My) and then held at that value. This was implemented by shifting the slopes shown in panel A up the y axis and does not mean that a constant SiW rate was prescribed (see text for details). Individual simulations are color-coded according to the slope of the relationships shown in panels *A* and *B*, where yellow lines represent models with a steeper SiW–CO_2 and shallower Ω_c–$CaCO_3$ export slope. It is not possible to change $[Ca^{2+}_{sw}]$ by perturbing the model in this way alone. (*D*, *G*, *J*, and *M*) Equivalent simulations in which $[Ca^{2+}_{sw}]$ was directly forced at a rate approximately equivalent to the Neogene rate of change (Fig. 1*A*). In simulations with a shallow SiW–CO_2 slope, pCO_2 decreases by up to ~800 ppmv. (*E*, *H*, *K*, and *N*) Equivalent simulations in which SiW was perturbed along with the $[Ca^{2+}]$ of the SiW product to a degree necessary to drive a twofold $[Ca^{2+}_{sw}]$ decrease.

increase in the weathering alkalinity flux to the ocean is counteracted by an increased $CaCO_3$ burial rate. Given that $[Ca^{2+}_{sw}]$ is less sensitive than the seawater carbonate system to changes in $CaCO_3$ burial ($[Ca^{2+}_{sw}]$/DIC = ~10 in the Eocene), a new equilibrium is achieved long before substantial changes in $[Ca^{2+}_{sw}]$ can occur, via the effect the carbonate chemistry change has on $CaCO_3$ burial (maximum ΔCa^{2+}_{sw} in these simulations is ~2.5%).

The second emergent model property is that all individual simulations fall on a single ΔpCO_2–ΔTAlk relationship, that is, none of the processes included in the model can result in a decoupling of TAlk and pCO_2 at the end of the model run (Fig. 4). Simulations with a steep SiW–CO_2 relationship result in a smaller TAlk and pCO_2 change, because those with a steeper SiW–CO_2 relationship return to equilibrium in response to a change in SiW more quickly

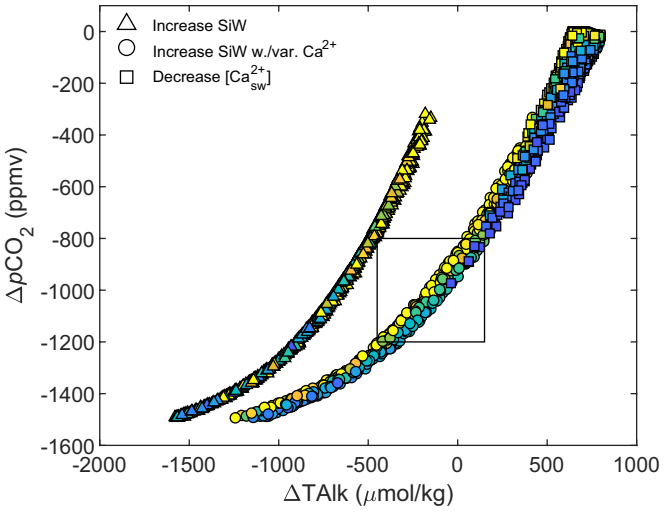

Fig. 4. The difference between the start and end pCO_2 and TAlk in the *DeepCarb* simulations shown in Fig. 3. Color is shown as a function of the individual simulation SiW–CO_2 and Ω_c-$CaCO_3$ export parameterizations; yellow symbols depict those with steeper SiW–CO_2 and shallower Ω_c-$CaCO_3$ slopes, respectively, and blue symbols the opposite; see Fig. 3 *A* and *B* for details. It is not possible to model the observed Cenozoic change in both pCO_2 and TAlk (black box; Fig. 2) unless $[Ca^{2+}_{sw}]$ is externally forced.

and with a lower overall change in pCO_2. The corollary of this is that, irrespective of the way in which the model parameterizations are implemented, if SiW is forced to match the model outcome to a known past change in CO_2, the associated TAlk change will always be the same. That is, although models with a steeper SiW–pCO_2 relationship would require a larger weathering forcing to result in a given ΔpCO_2, the resulting TAlk change would be virtually the same as an otherwise identical model with a shallower SiW–CO_2 slope and smaller forcing.

While a model perturbed in this way demonstrates the potential for long-term SiW (5) or CO_2 degassing rate changes (42) to be the sole explanation of the Cenozoic pCO_2 decrease, in all of these simulations, TAlk decreases to a far greater degree for a given pCO_2 change than is plausible based on our reconstruction (Fig. 2). Coupled with the inability of SiW/CO_2 changes in isolation to drive $[Ca^{2+}_{sw}]$, this hypothesized driver, at the very least, necessitates a strong additional driver of ocean alkalinity (in the opposite direction) and an alternative coincident mechanism of driving the observed $[Ca^{2+}_{sw}]$ change.

Externally forcing $[Ca^{2+}_{sw}]$ at a rate consistent with our Cenozoic record, while allowing all other model parameters to vary, invariably drives down pCO_2 while the change takes place, irrespective of how silicate weathering and calcification in the surface ocean are parameterized (Fig. 3*G*). This pCO_2 decrease results from a decrease in $CaCO_3$ burial (Fig. 3*M*), which initially occurs due to a lower Ω_c, as the effect of $[Ca^{2+}_{sw}]$ on Ω_c outweighs the resulting pH increase. Because the lower $CaCO_3$ burial rate drives both the surface and deep ocean to higher pH, net CO_2 diffusion from the atmosphere to the ocean takes place. This direct CO_2 flux to the ocean outweighs CO_2 accumulation in the atmosphere as silicate weathering rates decrease in response to the lower temperature/pCO_2.

This finding demonstrates a plausible mechanism by which a change in $[Ca^{2+}_{sw}]$ can exert a significant control on pCO_2 and indicates that the observed relationship between $[Ca^{2+}_{sw}]$ and pCO_2 (Fig. 2) *might* be causal. However, we again stress that, as with all model results presented here, the degree to which this is the case depends on how the key model relationships are parameterized. Specifically, the response of the model to a forced 10 mM $[Ca^{2+}_{sw}]$ decrease when allowed to equilibrate for 7 My after the perturbation strongly depends on how the silicate weathering–temperature relationship is parameterized, and to a lesser degree on whether there is a calcification response to Ω_c in the surface ocean. Models with a steep SiW–CO_2 slope ultimately return close to preperturbation CO_2, as an initial SiW decrease causes an imbalance between CO_2 outgassing and silicate weathering, and $CaCO_3$ burial rates reduce (Fig. 3*M*). Determining the degree to which $[Ca^{2+}_{sw}]$ may have driven CO_2 therefore depends on constraining the SiW-CO_2 slope. In contrast, models with a shallow SiW–CO_2 sensitivity and a surface ocean Ω_c feedback maintain substantially lower CO_2 because the $CaCO_3$ burial rate is maintained at its preperturbation level as a result of a small increase in deep ocean Ω_c. This occurs because the pH-driven $[CO_3^{2-}]$ increase ultimately outweighs the $[Ca^{2+}_{sw}]$ decrease (note that this relatively minor change is not at odds with the assumption of constant $\Omega_c \pm 0.5$ that forms the basis of the carbonate chemistry record presented in Figs. 1 and 2).

Finally, driving SiW and $[Ca^{2+}_{sw}]$ by covarying the Ca^{2+}/HCO_3^- of the weathering product (Fig. 3*E*) results in a set of simulations that more closely match the empirical results shown in Fig. 2. In this model, pCO_2 is more sensitive to SiW and TAlk remains stable in the simulations most closely matching the observed CO_2 change (Fig. 4) compared to forcing SiW alone. Overall, the results of this exercise are intermediate between the two endmember scenarios described above in which SiW and $[Ca^{2+}_{sw}]$ were driven independently. Greater degrees of pCO_2 change occur for a given SiW slope compared to the simulations in which SiW alone was forced (compare Fig. 3 *F* and *H*), demonstrating that both the change in SiW and the change in $[Ca^{2+}_{sw}]$ driven by SiW are responsible for a portion of the resulting pCO_2 decrease.

Our simple model cannot address which of the above scenarios is more likely, but it does produce results that are testable with our dataset. In all sets of model simulations presented here, the change in pCO_2 and TAlk at the end of the perturbation and equilibrium period fall onto a single relationship (Fig. 4). Crucially, simulations in which $[Ca^{2+}_{sw}]$ was forced, either indirectly by changing the Ca^{2+}/HCO_3^- of the weathering product or directly by changing $[Ca^{2+}_{sw}]$ alone, are characterized by a CO_2–TAlk relationship that is shifted to substantially higher TAlk for a given CO_2 (compare simulations represented by triangles and squares in Fig. 4). This is because as $[Ca^{2+}_{sw}]$ decreases, the $CaCO_3$ burial rate decreases relative to simulations in which no $[Ca^{2+}_{sw}]$ change take place, and alkalinity "accumulates" in the ocean. As such, models with a shallow SiW–temperature sensitivity and calcification feedback maintain approximately constant TAlk (Fig. 3*K*). Our carbonate system reconstruction demonstrates a minor decrease in TAlk over the Cenozoic (Fig. 2*A*), potentially adding evidence that a $[Ca^{2+}_{sw}]$-driven change in $CaCO_3$ burial rates, coupled with silicate weathering forcing the system in the opposite direction, is the mechanism which has acted to maintain ocean alkalinity at an approximately constant concentration throughout much of the Cenozoic (Fig. 3*K*) , in agreement with the findings of ref. 52. Nonetheless, we stress that this finding does not preclude other processes from acting as a TAlk or DIC feedback, such as the sensitivity of coccolithophore calcification to $[HCO_3^-]$ (53). We also stress that the rates described above refer to relatively minor changes that result in substantial shifts in seawater carbonate chemistry on multi-million-year timescales. As such, our hypothesis that pCO_2 is mechanistically coupled to $[Ca^{2+}_{sw}]$ via small (percent-level) changes in the $CaCO_3$ burial rate over millions of years is consistent with the observation that climate and the carbonate compensation depth (CCD) were decoupled through the early Cenozoic (54).

Given that we demonstrate a process by which $[Ca^{2+}_{sw}]$ may drive changes in ocean-atmosphere carbon partitioning (see also ref. 48 for a closely related hypothesis), our results highlight that changing seawater major ion chemistry is likely responsible for some of the Cenozoic pCO_2 decline. The degree to which this was the case remains an open question: addressing it is predicated in particular on determining the slope of the relationship between silicate weathering and climate and how it has varied across geologic time. In the simulations presented here with the strongest weathering–climate relationship, a pCO_2 change driven by weathering or degassing is almost entirely controlled by these processes, irrespective of whether or not $[Ca^{2+}_{sw}]$ is forced to match our reconstruction. In those with a shallower silicate weathering slope, the system is sufficiently dynamic that $[Ca^{2+}_{sw}]$ can do some of the "work." Determining where on this spectrum the Earth system lies is a necessary step in understanding the important drivers of the Cenozoic CO_2 decline, but our results suggest that unless the existence of a very responsive silicate weathering feedback can be demonstrated across multi-million-year timescales as well as across transient events (16), a substantial portion of the observed CO_2 decline is likely to have been driven by the large $[Ca^{2+}_{sw}]$ change that we show to have taken place.

Drivers of Seawater Major Ion Chemistry. Whether or not $[Ca^{2+}_{sw}]$ played a major role in driving CO_2, a key question is: what drove the change in $[Ca^{2+}_{sw}]$? While our data alone cannot provide this constraint, advances have recently been made in determining changes in seafloor spreading rates over the Neogene, with evidence for a ~40% decrease over the last 15 My (34). The close correspondence between the spreading rate data and our composite $[Ca^{2+}_{sw}]$ record (Fig. 1*D*) suggests that seawater–basalt interaction associated with mid-ocean ridge hydrothermal systems was a likely driver of seawater chemistry, given that these systems would have driven the observed major ion changes in the observed directions (44). Decreasing $[Ca^{2+}_{sw}]$ by ~10 mmol/kg over ~10 My requires the net removal of 1.4×10^9 moles calcium per year. While feedbacks are evidently in place to prevent changes in the hydrothermal flux from acting alone (e.g., $CaCO_3$ burial; see the previous section), this is a small fraction of the present-day flux (55) and thus readily reconcilable with the notion that the global seafloor spreading rate in the Neogene is responsible for this change.

Our composite seawater chemistry reconstruction indicates that, in the Neogene, the absolute magnitude of the $[Ca^{2+}_{sw}]$ change is approximately equal and opposite to that of $[Mg^{2+}_{sw}]$ (Fig. 1). The excess calcium concentration of hydrothermal fluids, i.e., that above the seawater concentration, is broadly equal to $[Mg^{2+}_{sw}] - [SO_4^{2-}]$, as anhydrite precipitation occurs in hydrothermal systems until SO_4^{2-} is completely removed and endmember hydrothermal fluid contains no Mg^{2+}, thus requiring charge balance via the release of Ca^{2+} (equation 1, ref. 56). This is equal to 26 to 29 mmol/kg in the Paleogene and early Neogene (~40 minus 14 mmol/kg; Fig. 1), assuming invariant $[Ca^{2+}_{sw}]\cdot[SO_4^{2-}{}_{sw}]$ as described above. This constrains Cenozoic hydrothermal systems to removing Mg^{2+} and releasing Ca^{2+} in a ratio of ~1.6 to 2.1, with the upper range representative of the modern ocean. While this is substantially greater than the value of 1 which would be required to result in the observation discussed above regarding Plio-Pleistocene Mg/Ca_{sw} (our finding that $\Delta[Ca^{2+}_{sw}] \sim= -\Delta[Mg^{2+}_{sw}]$), the magnitude of Plio-Pleistocene seawater chemistry change means that although the predicted $[Mg^{2+}_{sw}]$ increase is greater than that which we reconstruct, this discrepancy may simply be hidden within the uncertainty of the Mg^{2+}_{sw} data. Over longer periods this is not the case, given the larger magnitude of absolute change, thus requiring additional drivers of seawater chemistry given (e.g.) that $[Ca^{2+}_{sw}]$ and $[Mg^{2+}_{sw}]$ evolve in the same direction during the early Eocene. Likely candidates are changes in the rate of authigenic clay formation (23) and/or dolomitization (57) which have been suggested to have acted as additional Mg^{2+} sinks to a greater extent in the Paleogene than today, and could therefore conceivably provide part of the explanation for our reconstructed early Eocene $[Mg^{2+}_{sw}]$ decrease. A change in the Mg/Ca of weathered silicate rocks and/or greater interaction between seawater and mantle-derived mafic rocks along slow-spreading ridges (58) is consistent with the broad trends in our data. We note that the former process represents an additional possible driver of the Neogene pCO_2 decrease, within the framework of the notion that the emplacement of weatherable (ultramafic) material into the tropics impacted global silicate weathering rates (7), while the latter aligns with the observation that the Neogene decrease in crustal production is largely driven by a decrease in the length of fast-spreading ridges (34).

Notwithstanding the potential importance of a change in the silicate weathering rate independent of climate (i.e., emplacement or uplift), our new geochemical records combined with carbon cycle box modeling suggest that $[Ca^{2+}_{sw}]$ is a potential CO_2 driver. Together with the likely role of hydrothermal processes in explaining a large portion of the major element records presented here, this implies, for example, that the Neogene decrease in the seafloor spreading rate (34) resulted in a pCO_2 decrease via two mechanisms: directly via the associated decrease in CO_2 degassing (42), which is probably insufficient in isolation to explain all of the change, and indirectly via the impact that spreading rate has on seawater $[Ca^{2+}_{sw}]$, serving as a positive feedback (56). If $[Ca^{2+}_{sw}]$ has indeed causally driven pCO_2 via the mechanism outlined above, then this result could suggest that submarine hydrothermal processes are an important driver of long-term climate change and, by implication, that other factors are less important than previously thought.

Materials and Methods

The Paleogene seawater chemistry reconstructions presented here are based on exceptionally well-preserved fossil specimens of the larger benthic foraminifera *Nummulites* (including *Palaeonummulites*), with empirical calibrations performed using Recent *Operculina ammonoides*, the nearest living relative of this fossil genus. Coeval mid Eocene *Operculina* and *Nummulites* are known from one of the sites investigated here, with no resolvable offset in trace element incorporation between the two nummulitid foraminifera (59), which means that modern laboratory calibrations can be applied to the fossil samples with confidence.

The dataset is derived from globally distributed sites from five regions: northwest Europe, Java (Indonesia), Kutch (India), Tanzania (via the Tanzania Drilling Project), and the southeast United States (*SI Appendix*, Table S1). A subset of the samples reported here was previously analyzed for their clumped isotope composition (31). These regions were targeted for their exceptional carbonate fossil preservation, with all samples reported here having a glassy appearance under optical microscopy. The majority of the samples come from clay-rich horizons that have undergone shallow burial to much less than 100 °C. Sample preservation was assessed on an individual specimen basis through optical and electron microscopy, alongside measurements of trace elements diagnostic of different types of diagenesis (*SI Appendix*). In addition to the lack of any evidence of diagenetic bias of the proxy trace element data reported in the main text, the fact that our reconstructions are derived from five globally spaced sites adds further support to the integrity of the record, as the results are reproducible when derived from different nummulitid species from distinct basins with different depositional histories.

Fossil foraminifera were analyzed for element/Ca ratios by laser ablation ICPMS as described in refs. 59 and 60. Fossil samples were ultrasonicated in methanol twice, then three times in deionized water. The majority of samples were analyzed nondestructively, by mounting specimens vertically in the laser ablation chamber to facilitate multiple repeat depth profiling analyses through

the marginal cord. Material from a small number of the sample sites were embedded in resin and sectioned to enable the laser to be tracked across the entirety of the marginal cord. We observe no difference in the mean measured ratios by the two sampling strategies. Specimens were analyzed at Royal Holloway University of London (RHUL) using a RESOlution M-50 laser ablation system connected to either an Agilent 7500ce or 8800 ICPMS (61). For the purposes of the relatively high concentration trace element data discussed here, there was no difference in data quality between the two mass spectrometers. Most specimens were analyzed by slow (2 Hz) depth profiling of multiple ablation points on the marginal cord with a circular beam of 44 μm diameter (*SI Appendix*, Table S2); see ref. 59 for analytical details of samples that were embedded and sectioned. Ablation took place in a He atmosphere with 8.5 mL/min H_2 added as the additional diatomic gas to improve the ^{55}Mn limit of detection (60). Primary standardization was achieved via bracketing analyses of NIST SRM612, excepting Mg/Ca which was calibrated using the komatiite glass GOR132-G as it has a [Mg] far more comparable to these high-Mg foraminifera. Na/Ca, Mg/Ca, and Sr/Ca precision are all <5%, Mg/Ca and Sr/Ca accuracy were <2%, and Na/Ca accuracy <5% based on repeat analyses of the standard reference materials MPI-DING GOR132-G and MACS-3NP.

Data, Materials, and Software Availability. Code required to perform data analysis and produce the figures data have been deposited in Zenodo (62). All other data are included in the article and/or supporting information.

ACKNOWLEDGMENTS. D.E. and H.P.A. acknowledge the support from Yale University and D.E. acknowledges the support from the Royal Society (award reference URF\R1\221735) and UKRI [UKRI Frontier Research Guarantee Proposal (Horizon Europe ERC Starting Grants Guarantee)], award reference EP/Y034252/1. Part of this work was funded by NSF-BSF grant 2016534 to J.E. and Y.R., and by ISF grant 790/16 to J.E. Laser-ablation ICPMS work at RHUL was partly funded by a 2014 Natural Environment Research Council (NERC) Capital Equipment Grant (Ref. CC073) to W.M. The Tanzania Drilling Project was supported through NERC grants NE/X509345/1 and NE/B503225/1 and the Tanzania Petroleum Development Corporation.

Author affiliations: [a]School of Ocean and Earth Science, University of Southampton, Southampton SO14 3ZH, United Kingdom; [b]Department of Marine Sciences, Rutgers University, New Brunswick, NJ 08901; [c]Department of Earth and Planetary Sciences, Rutgers University, Piscataway, NJ 08854; [d]Institute of Earth Sciences, The Hebrew University of Jerusalem, Jerusalem 91904, Israel; [e]Israel Oceanographic and Limnological Research, National Institute of Oceanography, Haifa 3102201, Israel; [f]Natural History Museum Denmark, Sølvgade 83, København 1307, Denmark; [g]School of Ocean and Earth Science, Tongji University, Shanghai 200092, China; [h]Institute of Geosciences, Goethe University Frankfurt, Frankfurt am Main 60438, Germany; [i]Department of Earth and Environmental Sciences, Katholieke Universiteit Leuven, Leuven B-3000, Belgium; [j]Operational Directorate Earth and History of Life, Royal Belgian Institute of Natural Sciences, Brussels B-1000, Belgium; [k]Department of Earth Sciences, University College London, London WC1E 6BS, United Kingdom; [l]Naturalis Biodiversity Center, Leiden 2300 RA, The Netherlands; [m]Institute for Biodiversity and Ecosystem Dynamics, University of Amsterdam, Amsterdam 1098 XH, The Netherlands; [n]Department of Earth Sciences, Indian Institute of Technology Bombay, Mumbai 400076, India; and [o]Natural History Museum, London SW7 5BD, United Kingdom

1. D. Evans, J. Brugger, G. N. Inglis, P. Valdes, The temperature of the deep ocean is a robust proxy for global mean surface temperature during the Cenozoic. *Paleoceanogr. Paleoclimatol.* **39**, e2023PA004788 (2024).
2. G. N. Inglis *et al.*, Global mean surface temperature and climate sensitivity of the early Eocene Climatic Optimum (EECO), Paleocene-Eocene Thermal Maximum (PETM), and latest Paleocene. *Clim. Past* **16**, 1953–1968 (2020).
3. J. W. B. Rae *et al.*, Atmospheric CO_2 over the past 66 million years from marine archives. *Annu. Rev. Earth Planet. Sci.* **49**, 609–641 (2021).
4. B. Hönisch *et al.*; The Cenozoic CO_2 Proxy Integration Project (CENCO$_2$PIP) Consortium, Toward a Cenozoic history of atmospheric CO_2. *Science* **382**, eadi5177 (2023).
5. M. E. Raymo, W. F. Ruddiman, Tectonic forcing of late Cenozoic climate. *Nature* **359**, 117–122 (1992).
6. J. K. Caves Rugenstein, D. E. Ibarra, F. von Blanckenburg, Neogene cooling driven by land surface reactivity rather than increased weathering fluxes. *Nature* **571**, 99–102 (2019).
7. Y. Park *et al.*, Emergence of the Southeast Asian islands as a driver for Neogene cooling. *Proc. Natl. Acad. Sci. U.S.A.* **117**, 25319–25326 (2020).
8. O. Jagoutz, F. A. Macdonald, L. Royden, Low-latitude arc–continent collision as a driver for global cooling. *Proc. Natl. Acad. Sci. U.S.A.* **113**, 4935–4940 (2016).
9. G. Li, J. Ji, J. Chen, D. B. Kemp, Evolution of the Cenozoic carbon cycle: The roles of tectonics and CO_2 fertilization. *Glob. Biogeochem. Cycles* **23**, 2008GB003220 (2009).
10. N. Komar, R. E. Zeebe, Reconciling atmospheric CO_2, weathering, and calcite compensation depth across the Cenozoic. *Sci. Adv.* **7**, eabd4876 (2021).
11. A. Ridgwell, A mid mesozoic revolution in the regulation of ocean chemistry. *Mar. Geol.* **217**, 339–357 (2005).
12. R. A. Berner, K. Caldeira, The need for mass balance and feedback in the geochemical carbon cycle. *Geology* **25**, 955–956 (1997).
13. T. Tyrrell, Chance played a role in determining whether Earth stayed habitable. *Commun. Earth Environ.* **1**, 1–10 (2020).
14. J. M. Edmond, Y. Huh, Non-steady state carbonate recycling and implications for the evolution of atmospheric pCO_2. *Earth Planet. Sci. Lett.* **216**, 125–139 (2003).
15. R. A. Berner, A. C. Lasaga, R. M. Garrels, Carbonate-silicate geochemical cycle and its effect on atmospheric carbon dioxide over the past 100 million years. *Am. J. Sci.* **283**, 641–683 (1983).
16. P. A. E. Pogge von Strandmann *et al.*, Lithium isotope evidence for enhanced weathering and erosion during the Paleocene-Eocene thermal maximum. *Sci. Adv.* **7**, eabh4224 (2021).
17. D. E. Penman, Silicate weathering and North Atlantic silica burial during the Paleocene-Eocene thermal maximum. *Geology* **44**, 731–734 (2016).
18. D. E. Penman, J. K. Caves Rugenstein, D. E. Ibarra, M. J. Winnick, Silicate weathering as a feedback and forcing in Earth's climate and carbon cycle. *Earth-Sci. Rev.* **209**, 103298 (2020).
19. R. G. Hilton, A. J. West, Mountains, erosion and the carbon cycle. *Nat. Rev. Earth Environ.* **1**, 284–299 (2020).
20. M. Pagani, K. Caldeira, R. Berner, D. J. Beerling, The role of terrestrial plants in limiting atmospheric CO_2 decline over the past 24 million years. *Nature* **460**, 85–88 (2009).
21. T. K. Lowenstein, M. N. Timofeeff, S. T. Brennan, L. A. Hardie, R. V. Demicco, Oscillations in phanerozoic seawater chemistry: Evidence from fluid inclusions. *Science* **294**, 1086–1088 (2001).
22. S. T. Brennan, T. K. Lowenstein, D. I. Cendón, The major-ion composition of Cenozoic seawater: The past 36 million years from fluid inclusions in marine halite. *Am. J. Sci.* **313**, 713–775 (2013).
23. J. A. Higgins, D. P. Schrag, The Mg isotopic composition of Cenozoic seawater–Evidence for a link between Mg-clays, seawater Mg/Ca, and climate. *Earth Planet. Sci. Lett.* **416**, 73–81 (2015).
24. C. Langdon *et al.*, Effect of calcium carbonate saturation state on the calcification rate of an experimental coral reef. *Glob. Biogeochem. Cycles* **14**, 639–654 (2000).
25. D. Evans, W. Müller, Deep time foraminifera Mg/Ca paleothermometry: Nonlinear correction for secular change in seawater Mg/Ca. *Paleoceanography* **27**, 2012PA002315 (2012).
26. C. Lécuyer, Seawater residence times of some elements of geochemical interest and the salinity of the oceans. *Bull. Soc. Géol. France* **187**, 245–260 (2016).
27. H. Hauzer, D. Evans, W. Müller, Y. Rosenthal, J. Erez, Calibration of Na partitioning in the calcitic foraminifer *Operculina ammonoides* under variable Ca concentration: Toward reconstructing past seawater composition. *Earth Planet. Sci. Lett.* **497**, 80–91 (2018).
28. R. E. Zeebe, T. Tyrrell, History of carbonate ion concentration over the last 100 million years II: Revised calculations and new data. *Geochim. Cosmochim. Acta* **257**, 373–392 (2019).
29. X. Zhou *et al.*, Planktic foraminiferal Na/Ca: A potential proxy for seawater calcium concentration. *Geochim. Cosmochim. Acta* **305**, 306–322 (2021).
30. C. H. Lear, H. Elderfield, P. A. Wilson, A cenozoic seawater Sr/Ca record from benthic foraminiferal calcite and its application in determining global weathering fluxes. *Earth Planet. Sci. Lett.* **208**, 69–84 (2003).
31. D. Evans *et al.*, Eocene greenhouse climate revealed by coupled clumped isotope-Mg/Ca thermometry. *Proc. Natl. Acad. Sci. U.S.A.* **115**, 1174–1179 (2018).
32. L. J. Cotton, D. Evans, S. Beavington-Penney, The high-magnesium calcite origin of nummulitid foraminifera and implications for the identification of calcite diagenesis. *Palaios* **35**, 421–431 (2020).
33. D. Evans, C. Brierley, M. E. Raymo, J. Erez, W. Müller, Planktic foraminifera shell chemistry response to seawater chemistry: Pliocene–Pleistocene seawater Mg/Ca, temperature and sea level change. *Earth Planet. Sci. Lett.* **438**, 139–148 (2016).
34. C. A. Dalton, D. S. Wilson, T. D. Herbert, Evidence for a global slowdown in seafloor spreading since 15 Ma. *Geophys. Res. Lett.* **49**, 2022GL097937 (2022).
35. R. D. Müller *et al.*, Solid earth carbon degassing and sequestration since 1 billion years ago. *Geochem. Geophys. Geosyst.* **25**, e2024GC011713 (2024).
36. S. M. Stanley, L. A. Hardie, Secular oscillations in the carbonate mineralogy of reef-building and sediment-producing organisms driven by tectonically forced shifts in seawater chemistry. *Palaeogeogr. Palaeoclimatol. Palaeoecol.* **144**, 3–19 (1998).
37. J. Horita, H. Zimmermann, H. D. Holland, Chemical evolution of seawater during the Phanerozoic: Implications from the record of marine evaporites. *Geochim. Cosmochim. Acta* **66**, 3733–3756 (2002).
38. T. J. Algeo, G. M. Luo, H. Y. Song, T. W. Lyons, D. E. Canfield, Reconstruction of secular variation in seawater sulfate concentrations. *Biogeosciences* **12**, 2131–2151 (2015).
39. E. Anagnostou *et al.*, Changing atmospheric CO_2 concentration was the primary driver of early Cenozoic climate. *Nature* **533**, 380–384 (2016).
40. J. C. Zachos *et al.*, Rapid acidification of the ocean during the Paleocene-Eocene thermal maximum. *Science* **308**, 1611–1615 (2005).
41. F. A. Macdonald, N. L. Swanson-Hysell, Y. Park, L. Lisiecki, O. Jagoutz, Arc-continent collisions in the tropics set Earth's climate state. *Science* **364**, 181–184 (2019).
42. T. D. Herbert *et al.*, Tectonic degassing drove global temperature trends since 20 Ma. *Science* **377**, 116–119 (2022).
43. T. J. Wolery, N. H. Sleep, Hydrothermal circulation and geochemical flux at mid-ocean ridges. *J. Geol.* **84**, 249–275 (1976).
44. R. M. Coggon, D. A. H. Teagle, C. E. Smith-Duque, J. C. Alt, M. J. Cooper, Reconstructing past seawater Mg/Ca and Sr/Ca from mid-ocean ridge flank calcium carbonate veins. *Science* **327**, 1114–1117 (2010).
45. H. de Moel *et al.*, Planktic foraminiferal shell thinning in the Arabian Sea due to anthropogenic ocean acidification? *Biogeosciences* **6**, 1917–1925 (2009).
46. J. Erez, S. Reynaud, J. Silverman, K. Schneider, D. Allemand, "Coral calcification under ocean acidification and global change" in *Coral Reefs: An Ecosystem in Transition*, Z. Dubinsky, N. Stambler, Eds. (Springer Netherlands, 2011), pp. 151–176.
47. S. R. Emerson *et al.*, Calcium carbonate preservation in the ocean. *Philos. Trans. R. Soc. Lond. Series A Math. Phys. Sci.* **331**, 29–40 (1997).
48. G. A. Shields, B. J. W. Mills, Evaporite weathering and deposition as a long-term climate forcing mechanism. *Geology* **49**, 299–303 (2020).
49. J. K. Caves, A. B. Jost, K. V. Lau, K. Maher, Cenozoic carbon cycle imbalances and a variable weathering feedback. *Earth Planet. Sci. Lett.* **450**, 152–163 (2016).

50. L. A. Coogan, S. E. Dosso, Alteration of Ocean crust provides a strong temperature dependent feedback on the geological carbon cycle and is a primary driver of the Sr-isotopic composition of seawater. *Earth Planet. Sci. Lett.* **415**, 38–46 (2015).
51. K. Deng, S. Yang, Y. Guo, A global temperature control of silicate weathering intensity. *Nat. Commun.* **13**, 1781 (2022).
52. W. Si, T. Herbert, M. Wu, Y. Rosenthal, Increased biogenic calcification and burial under elevated pCO_2 during the miocene: A model-data comparison. *Global Biogeochem. Cycles* **37**, e2022GB007541 (2023).
53. L. T. Bach, U. Riebesell, M. A. Gutowska, L. Federwisch, K. G. Schulz, A unifying concept of coccolithophore sensitivity to changing carbonate chemistry embedded in an ecological framework. *Prog. Oceanogr.* **135**, 125–138 (2015).
54. S. E. Greene *et al.*, Early cenozoic decoupling of climate and carbonate compensation depth trends. *Paleoceanogr. Paleoclimatol.* **34**, 930–945 (2019).
55. H. Elderfield, A. Schultz, Mid-ocean ridge hydrothermal fluxes and the chemical composition of the ocean. *Annu. Rev. Earth Planet. Sci.* **24**, 191–224 (1996).
56. M. A. Antonelli, N. J. Pester, S. T. Brown, D. J. DePaolo, Effect of paleoseawater composition on hydrothermal exchange in midocean ridges. *Proc. Natl. Acad. Sci. U.S.A.* **114**, 12413–12418 (2017).
57. P. A. E. Pogge von Strandmann, J. Forshaw, D. N. Schmidt, Modern and Cenozoic records of seawater magnesium from foraminiferal Mg isotopes. *Biogeosciences* **11**, 5155–5168 (2014).
58. M. Ligi, E. Bonatti, M. Cuffaro, D. Brunelli, Post-Mesozoic rapid increase of seawater Mg/Ca due to enhanced mantle-seawater interaction. *Sci. Rep.* **3**, 2752 (2013).
59. D. Evans, W. Müller, S. Oron, W. Renema, Eocene seasonality and seawater alkaline earth reconstruction using shallow-dwelling large benthic foraminifera. *Earth Planet. Sci. Lett.* **381**, 104–115 (2013).
60. D. Evans, J. Erez, S. Oron, W. Müller, Mg/Ca-temperature and seawater-test chemistry relationships in the shallow-dwelling large benthic foraminifera *Operculina ammonoides*. *Geochim. Cosmochim. Acta* **148**, 325–342 (2015).
61. W. Müller, M. Shelley, P. Miller, S. Broude, Initial performance metrics of a new custom-designed ArF excimer LA-ICPMS system coupled to a two-volume laser-ablation cell. *J. Anal. At. Spectrom.* **24**, 209–214 (2009).
62. D. Evans *et al.*, Code and datasets to accompany Evans et al. (2025): The major ion chemistry of seawater was closely coupled to the long-term carbon cycle during the Cenozoic. Zenodo. https://doi.org/10.5281/zenodo.17783082. Deposited 12 January 2025.